IEEE Access
Multidisciplinary | Rapid Review | Open Access Journal

Received November 25, 2017, accepted December 13, 2017, date of publication December 27, 2017, date of current version March 15, 2018.

Digital Object Identifier 10.1109/ACCESS.2017.2785406

Fault Detection Based on a Bio-Inspired Vibration Sensor System

ZHENGCHAO LI[1,2], XINGJIAN JING[1,3], (Senior Member, IEEE), AND JINYONG YU[2]

[1]Department of Mechanical Engineering, The Hong Kong Polytechnic University, Hong Kong 999077
[2]Research Institute of Intelligent Control and System, Harbin Institute of Technology, Harbin 150001, China
[3]The Hong Kong Polytechnic University Shenzhen Research Institute, Shenzhen 518057, China

Corresponding author: Xingjian Jing (e-mail: xingjian.jing@polyu.edu.hk)

This work was supported in part by the General Research Fund Project of Research Grants Council of Hong Kong under Grant 15206717, in part by National Natural Science Foundation of China Projects under Grant 61374041 and Grant 61673133, and in part by the Internal Research Funds from The Hong Kong Polytechnic University. This paper was presented in part at the 2017 Asian Control Conference, December 17–20, 2017, Gold Coast, Australia.

ABSTRACT A novel vibration sensor based on a bio-inspired nonlinear structure with quasi-zero stiffness characteristic is developed for the real-time measurement of absolute vibration motion. With this bio-inspired vibration sensor, the problems of error accumulation and real-time performance induced by traditional measurement method using accelerometer can be effectively eliminated. In order to construct a comparatively exact model of the bio-inspired vibration sensor, an adaptive compensation method is applied to the estimation of the structure parameter. Through taking full advantage of the bio-inspired vibration sensor in real-time measurement of absolute vibration motion, a model-based fault detection algorithm is proposed to cope with the real-time detection problem of weak fault with fast time-varying characteristic which cannot be exactly identified by existing frequency-based and wavelet-based fault detection methods. Theoretical analysis and experimental results demonstrate that the fault detection algorithm based on this bio-inspired vibration sensor is effective and efficient, compared with the existing ones and thus has a great potential in many real practical applications.

INDEX TERMS Bio-inspired vibration sensor, real-time measurement of absolute motion, vibration-based fault detection.

I. INTRODUCTION

Vibration analysis is one of the fundamental condition monitoring techniques for machinery maintenance and fault diagnosis, which can be used in the cases of manufacturing and operating to realize the quality control and health monitoring. During past decades, a series of significant results on vibration-based fault diagnosis have been reported in various fields of industrial applications, such as railway wheel flat fault detection [1], winding deformation detection of power grid transformer [2], [3], and structural damage detection of gear, bearing, stator and rotor in mechanical system [4]–[8]. A key factor of conducting fault detection is to acquire accurate vibration signals, including amplitude, velocity, and acceleration. For example, in power grid transformer, it is desired to use vibration motion to describe the degree of winding deformation. A general way is to use accelerometer as the measurement of vibration motion. Nevertheless, this solution will lead to serious problem of error accumulation due to double time-domain integration of the acceleration signal with non-zero mean. Especially, the accumulation error increases over the time. An alternative method is adopting frequency-domain integral instead of the time-domain. Through setting the corresponding low-frequency component generated from integral as zero, the accumulation can be cancelled. It is worth pointing out the frequency-domain integral requires a complete acceleration signal, which indicates that the frequency-domain integral can not be extended to real-time fault detection. Besides, some studies also use laser [9] to measure absolute motion, but which holding the strict requirements of installation space, environment, and cost is limited in some practical applications. Hence, an interesting and challenging topic arises naturally: *whether is it possible to simply and effectively realize the real-time measurement of absolute vibration motion by resorting to some novel measuring methods*? One of the purposes of this paper is to give a positive answer to the above question.

On the other hand, nonlinear structure with very beneficial nonlinear stiffness and damping characteristics has

received growing attention due to its excellent performance of achieving vibration isolation or suppression [10]–[14]. Some applications of nonlinear structure can be found in vibration isolator with quasi-zero stiffness (QZS) [11]–[13]. Recently, a novel nonlinear structure inspired by the limb structures of animals and insects in motion vibration control has been systematically investigated by Wu *et al.* [15], Jing *et al.* [16], and Pan *et al.* [17]. This novel structure is also called Z-like or X-like shape structure. The X-like shape structure can be regarded as the combination of Z-like shape structure. As shown in Fig. 1, the bird's leg is Z-like skeleton. Compared with existing QZS structures, this bio-inspired structure has better loading capacity and equilibrium stability. Meanwhile, this bio-inspired structure can be easily implemented with only linear spring and damper components.

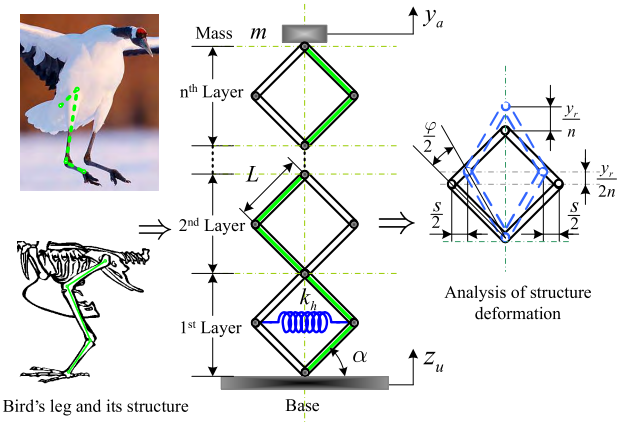

FIGURE 1. The structural mechanism inspired from the bird's leg.

Based on the previous discussion about bio-inspired structure, an attempt will be made to construct a bio-inspired vibration sensor for the accurate real-time measurement of absolute motion in this paper. It is known that this bio-inspired structure with QZS property can create an absolute stable point to acquire very excellent performance of vibration isolation or suppression. With this idea, the problem of measurement of absolute motion can be translated into the measurement of relative motion between the stable point and other vibrating points in bio-inspired vibration sensor. The relative motion can be easily measured by using various sensors such as optical encoder and grating ruler. Importantly, the measurement accuracy and bandwidth can be fulfilled conveniently through flexibly adjusting corresponding structural parameters. Hence, the problems of error accumulation and real-time from accelerometer measurement can be eliminated by utilizing the bio-inspired vibration sensor.

Although the fault detection techniques have been greatly developed [3]–[7] in the field of vibration-based analysis, there still exist some attractive and challenging topics worth further studying, one of which is how to detect the weak fault signal with fast time-varying characteristic from strong vibration in real time. For example, in vibration and shock testing platform, the weak fault may be masked in vibration signal. Existing frequency-domain based fault detection methods do not have the ability to identify it since the fast time-varying weak fault has almost no characterization on the spectrum. Multi-resolution wavelet-based method gives a positive answer to the detection problem of fast time-varying fault, which can be located by analysing the singular value of wavelet decomposition components. However, it is worth noting that the wavelet-based fault detection method is not real time. As aforementioned observations, this bio-inspired vibration sensor system has provided a simple and effective way for the real-time accuracy measurement of absolute motion, which makes the absolute motion based real-time fault detection possible. On the other side, the model-based method, which uses the soft redundancy instead of hardware redundancy to generate residual signal for decision making, has been wildly applied in the fault detection of practical systems [18]–[21]. Through combining this bio-inspired vibration sensor and model-based fault detection method, a real-time fault detection algorithm based on measurement of absolute motion is proposed.

The main contributions are summarized as follows:

(1) A novel vibration sensor based on bio-inspired nonlinear structure with QZS characteristic is developed for the real-time measurement of absolute vibration motion. The problems of error accumulation and real-time performance from traditional measurement method using accelerometer can be effectively eliminated by adopting this bio-inspired vibration sensor.

(2) An adaptive compensation method is applied to estimation of rotational damping coefficient, which can give a comparatively exact model of the bio-inspired vibration sensor.

(3) Through taking full advantage of the bio-inspired vibration sensor in real-time measurement of absolute vibration motion, a model based fault detection algorithm is designed to solve the real-time detection problem of weak fault with fast time-varying characteristic. A nonlinear observer is designed as the soft redundancy to generate the residual signal, which is sensitive to fault signal. In order to reliably identify the fault, the residual evaluation function is constructed based on sliding time-window norm.

The remainder of this paper is structured as follows. Section II starts with model description and analysis of the bio-inspired vibration sensor. In Section III, an adaptive compensation method is applied to the model construction. Base on the bio-inspired vibration sensor, Section IV presents an observer-based real-time fault detection algorithm. Some results are presented in Section V to demonstrate the effectiveness and applicability of the proposed methodologies. Finally, Section VI concludes the paper.

II. MODEL DESCRIPTION AND ANALYSIS

As depicted in Fig. 1, the n-layer bio-inspired vibration sensor system consists of connecting rods and rotating joints. This novel nonlinear structure is inspired by the limb structures of animals and insects in motion vibration control.

As shown in Fig. 1, the bird's leg is Z-like skeleton. With this Z-like shape structure, the bird's running and landing is very steady, even in a very high speed. That means this Z-like structure has the potential of suppressing the vibration. In practical system, the X-like shape structure, which can be regarded as the combination of double Z-like shape structures, is much easier to be implemented. A linear spring with horizontal stiffness in the bottom layer is used as passive muscles. All the parameter descriptions of the bio-inspired vibration sensor are listed in Tab. 1.

TABLE 1. Parameter descriptions of the bio-inspired sensor.

Symbol	Description
m	loading mass (kg)
L	length of rod (m)
α	initial angle (rad)
φ	rotational motion (rad)
s	horizontal motion (m)
n	number of layers
n_x	number of joints
k_h	linear spring stiffness (N/m)
c	rotational damping coefficient (N*s/rad)
y_a	absolute motion of the mass (m)
z_u	base excitation (m)
y_r	relative motion between mass and base (m)

Remark 1: This bio-inspired vibration sensor is mainly designed for measurement of absolute vertical motion. In practical structure, a support rod will be placed in the center line to limit the movement towards the vertical direction. Along these lines, the deformation on the bio-inspired vibration sensor is symmetrical. The dynamics can be modeled as a single degree of freedom system.

The relationships among φ, s, and y_r are described as

$$\varphi = 2\arctan\left(\frac{L\sin\alpha + \frac{y_r}{2n}}{L\cos\alpha - \frac{s}{2}}\right) - 2\alpha \tag{1}$$

$$s = 2L\cos\alpha - 2\sqrt{L^2 - (L\sin\alpha + \frac{y_r}{2n})^2} \tag{2}$$

Here, selecting the upward as the positive direction, the relative motion between the mass and base is $y_r = y_a - z_u$.

By resorting to Lagrange's method as in [15], the dynamics of such a bio-inspired sensor system is characterized by

$$\begin{aligned} m\ddot{y}_r + m\ddot{z}_u + k_h s\frac{ds}{dy_r} &= -c\,n_x\left(\frac{d\varphi}{dy_r}\right)^2\dot{y}_r \\ \frac{d\varphi}{dy_r} &= \frac{1}{n\sqrt{L^2 - (L\sin\alpha + \frac{y_r}{2n})^2}} \\ \frac{ds}{dy_r} &= \frac{L\sin\alpha + \frac{y_r}{2n}}{n\sqrt{L^2 - (L\sin\alpha + \frac{y_r}{2n})^2}} \end{aligned} \tag{3}$$

where $k_h\, s\frac{ds}{dy_r}$ and $c\,n_x\left(\frac{d\varphi}{dy_r}\right)^2\dot{y}_r$ are equivalent nonlinear stiffness and damping correspondingly. Notice that the equivalent nonlinear stiffness and damping come not from the nonlinear spring and/or damper but from the specially geometric relationship of this bio-inspired sensor structure, which is one of the obvious advantages.

As can be seen from (3), the equivalent nonlinear stiffness $k_h s\frac{ds}{dy_r}$ and damping coefficient $c\,n_x\left(\frac{d\varphi}{dy_r}\right)^2$ are rather complicated. For the convenience of analysis and design, the equivalent nonlinear stiffness and damping coefficient are represented as polynomial expressions through Taylor series expansion at zero equilibrium, which are given in Appendix A. The comparison results between exact value and Taylor expansion are illustrated in Fig. 2 and 3. Since the vertical motion of the bio-inspired sensor considered in this paper does not exceed 0.05 m as shown in Section V, the approximation accuracy is accepted in the rest analysis and design.

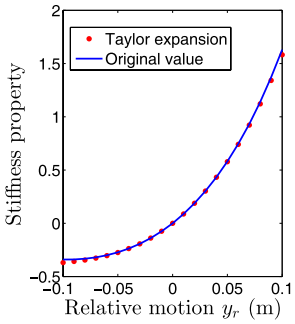

FIGURE 2. Comparison between exact value and Taylor expansion (stiffness).

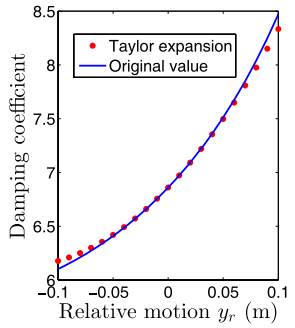

FIGURE 3. Comparison between exact value and Taylor expansion (damping).

Then, the resonant frequency of the bio-inspired vibration sensor system is

$$f_0 = \frac{\tan\alpha}{2n\pi}\sqrt{\frac{k_h}{m}} \tag{4}$$

The equivalent nonlinear stiffness (A.1) depends not only on the linear spring stiffness but also on the connecting rod length, initial angle, and lay number. This is the superiority of the bio-inspired structure, and also the fundamental distinction between the traditional mass-spring system and the bio-inspired structure of this paper. With the beneficial nonlinear stiffness, the low resonant frequency can be easily achieved through adjusting the structural parameters, upon which a wider frequency range with excellent vibration isolation or suppression performance can be guaranteed.

In addition, the equivalent nonlinear damping can make a positive contribution to improve the vibration isolation

TABLE 2. The effects of the structural parameters.

	Resonant frequency	Vibration transmissibility
Increasing L	—	↑
Increasing α	↑	↑
Increasing n	↓	↓
Increasing k_h	↑	↑
Increasing c	—	↓

or suppression performance. Generally, increasing the linear damping can suppress the resonant peak but also degrades the performance at high frequency range. This difficulty can also be settled by resorting to the equivalent nonlinear damping providing the strong damping at resonant region but weak damping at high frequency range. Thus, with the beneficial nonlinear stiffness and damping, this bio-inspired structure has excellent vibration isolation or suppression performance, as detailed discussion and analysis in [12], [15], and [16].

Remark 2: When the resonant frequency of the bio-inspired structure is sufficiently low, the QZS characteristic can be achieved in a very wide range of frequencies. With the QZS property, a very excellent performance of vibration isolation or suppression can be acquired. Then the top layer mass m is approximately equivalent to a stable anti-vibration point, i.e., the amplitude of y_a is close to zero and $z_u \approx -y_r$. Thus, the measurement of absolute motion z_u can be translated into the measurement of relative motion y_r between the stable anti-vibration point and the base in this bio-inspired vibration sensor. By resorting to some simple sensors such as optical encoder and grating ruler, the relative motion y_r can be easily measured. Furthermore, this bio-inspired vibration sensor can achieve desired measurement performance by tuning the structural parameters (e.g., connecting rod length, initial angle, layer number, spring stiffness, and loading mass). A simple description about the effects of the structural parameters on the performance of vibration isolation is summarized in Table 2. The symbol "—", "↑", and "↓" represent increase, decrease, and no change respectively. Actually, these structural parameters are strongly coupled through the geometrical nonlinearity. When designing structural parameters, tradeoff considerations must be executed according to the practical application. For example, a spring with smaller stiffness is selected to obtain lower resonant frequency and wider frequency range of vibration isolation or suppression, but the smaller stiffness will result in the significant degradation of loading capacity and cause a larger static displacement, thus the tradeoff between the vibration isolation/suppression performance and loading capacity should be taken into account.

Obviously, the relative motion y_r can be determined through measuring the rotation angle φ, which is implemented by installing an optical encoder in the bottom joint. The relationship between the rotation angle φ and the relative motion y_r is determined by

$$y_r = 2nL(\sin(\alpha + \frac{\varphi}{2}) - \sin(\alpha)) \tag{5}$$

Let $x_1(t) = y_r(t)$ and $x_2(t) = \dot{y}_r(t)$ be state variables, then the bio-inspired vibration sensor system (3) can be expressed as the following nonlinear state space equation

$$\dot{x}(t) = \begin{bmatrix} \dot{y}_r \\ -\frac{k_h}{m} s \frac{ds}{dy_r} - \frac{c}{m} n_x (\frac{d\varphi}{dy_r})^2 \dot{y}_r \end{bmatrix} + \begin{bmatrix} 0 \\ -1 \end{bmatrix} u(t) \tag{6}$$

where $x(t) = [x_1(t)\ x_2(t)]^T$ is state vector, $u(t) = \ddot{z}_u(t)$ is input signal.

Implementing the real-time measurement and fault detection requires the discrete time model of above sensor system, which is obtained according to the Euler discretization method and Taylor expansions as given in (A.1) and (A.2). For simple description, x_k^i is used to represent the i^{th} state at time instance k. And define $x_k^1 = y_r$, $x_k^2 = \dot{y}_r$.

$$x_{k+1} = Ax_k + D_f f(x_k) + Bu_k \tag{7}$$

where $f(x_k)$ is a nonlinear function of state variables,

$$\begin{aligned} &f(x_k) \\ &= \frac{3 \sin\alpha \sec^4\alpha\, k_h}{4 m L n^3} {y_r}^2 - \frac{(4 \sec^4\alpha - 5 \sec^6\alpha)\, k_h}{8 m L^2 n^4} {y_r}^3 \\ &\quad + c\, n_x\, \dot{y}_r \left(\frac{\sin\alpha \sec^4\alpha}{m L^3 n^3} y_r - \frac{(3 \sec^4\alpha - 4 \sec^6\alpha)}{4 m L^4 n^4} {y_r}^2 \right) \end{aligned} \tag{8}$$

T_s is the sampling period and

$$A = \begin{bmatrix} 1 & T_s \\ -\frac{\tan^2\alpha\, k_h\, T_s}{m n^2} & 1 - \frac{c\, n_x \sec^2\alpha\, T_s}{m L^2 n^2} \end{bmatrix}, \quad D_f = \begin{bmatrix} 0 \\ T_s \end{bmatrix}$$
$$B = \begin{bmatrix} 0 \\ -T_s \end{bmatrix} \tag{9}$$

III. PARAMETER ESTIMATION

In many mechanical systems, it is hard to directly get ideal knowledge on the structure parameter or the cost of measurement is probably expensive [22]–[26]. The same situation is encountered in this bio-inspired vibration sensor system. In order to obtain a comparatively exact model of the sensor system, an adaptive compensation method is applied to estimate the rotational damping coefficient [27].

For the convenience of estimating the damping coefficient, the bio-inspired sensor system (6) is reformulated as

$$x_{k+1} = x_k + F(x_k, u_k) + G(x_k, u_k)\theta \tag{10}$$

where $\theta = \frac{c}{m}$ is the parameter to be estimated, nonlinear functions $F(x_k, u_k)$ and $G(x_k, u_k)$ are defined as

$$F(x_k, u_k) = T_s \begin{bmatrix} x_k^2 \\ -\frac{k_h}{m} s \frac{ds}{dy_r} - u_k \end{bmatrix}$$
$$G(x_k, u_k) = T_s \begin{bmatrix} 0 \\ -n_x (\frac{d\varphi}{dy_r})^2 \dot{y}_r \end{bmatrix}$$

Construct the following state-predictor for sensor system (10)

$$\hat{x}_{k+1} = \hat{x}_k + F(x_k, u_k) + G(x_k, u_k)\theta_0 + \mathcal{K}(x_k - \hat{x}_k) \quad (11)$$

where θ_0 is the initial guess of unknown parameter θ and $\mathcal{K} > 0$ is the compensation coefficient. Let the state estimation error be $e_k = x_k - \hat{x}_k$. From sensor system (10) and state predictor (11), the state estimation error is provided by

$$e_{k+1} = e_k + G(x_k, u_k)(\theta - \theta_0) - \mathcal{K}e_k \quad (12)$$

Define auxiliary variables η_k and ω_k as

$$\eta_k = e_k - \omega_k(\theta - \theta_0) \quad (13)$$

$$\omega_{k+1} = \omega_k + G(x_k, u_k) - \mathcal{K}\omega_k, \quad \omega_0 = 0 \quad (14)$$

According to (12), (13) and (14), it is obtained that

$$\eta_{k+1} = \eta_k - \mathcal{K}\eta_k, \quad \eta_0 = e_0 \quad (15)$$

Let the parameter estimation error be $\tilde{\theta}_k = \theta - \hat{\theta}_k$. The dynamic can be presented as

$$\tilde{\theta}_{k+1} = \tilde{\theta}_k - \frac{1}{\|\mathcal{Q}_k\| + \varepsilon}(\mathcal{C}_k - \mathcal{Q}_k\hat{\theta}_k) \quad (16)$$

Assume that at a time step k_c, $\mathcal{Q}_{k_c} > 0$ is satisfied. This condition is equivalent to the standard persistently exciting condition stated in terms of the sum of $w_k^T w_k$ being positive definite over a finite interval of time [27]. Then, it follows from (13) and (22) that the following relationship holds $\forall k \geq k_c$

$$\mathcal{Q}_k\theta = \sum_{i=0}^{k} \omega_i^T \omega_i \theta = \sum_{i=0}^{k} \omega_i^T(\omega_i\theta_0 + e_i - \eta_i) = \mathcal{C}_k \quad (17)$$

Substituting $\mathcal{C}_k = \mathcal{Q}_k\theta$ into (18) yields

$$\tilde{\theta}_{k+1} = (I - \frac{\mathcal{Q}_k}{\|\mathcal{Q}_k\| + \varepsilon})\tilde{\theta}_k \quad (18)$$

where ε is a small scalar. Thus the parameter estimation error $\tilde{\theta}$ is decreasing $\forall k \geq k_c$, and $\lim_{k\to\infty} \tilde{\theta} = 0$.

Consequently, an algorithm for the damping coefficient estimation is summarized as follows.

Algorithm 1 Algorithm for Parameter Estimation

1: Give initial guess θ_0 and $\mathcal{K}$, set $k = 0$.

2: Calculate the state predictor (11) .

3: Calculate the auxiliary variables.

$$\eta_{k+1} := \eta_k - \mathcal{K}\eta_k, \eta_0 = e_0 \quad (19)$$

$$\omega_{k+1} := \omega_k + G(x_k, u_k) - \mathcal{K}\omega_k, \quad \omega_0 = 0 \quad (20)$$

$$\mathcal{Q}_{k+1} := \mathcal{Q}_k + \omega_k^T\omega_k, \quad \mathcal{Q}_0 = 0 \quad (21)$$

$$\mathcal{C}_{k+1} := \mathcal{C}_k + \omega_k^T(\omega_k\theta_0 + e_k - \eta_k), \quad \mathcal{C}_0 = 0 \quad (22)$$

4: Update parameter

$$\hat{\theta}_{k+1} := \hat{\theta}_k + \frac{1}{\|\mathcal{Q}_k\| + \varepsilon}(\mathcal{C}_k - \mathcal{Q}_k\hat{\theta}_k) \quad (23)$$

5: Set $k \leftarrow k + 1$, and go back to Stage 2.

Remark 3: In light of the above analysis, it is clear that the parameter estimation error will converge to zero exponentially when the persistently exciting condition is satisfied. The experiment of parameter estimation will be conducted in the ideal laboratory environment, therefore system state and excitation input can be measured exactly.

IV. APPLICATION ON FAULT DETECTION

The bio-inspired vibration sensor system has provided a simple and effective way for the real-time measurement of absolute motion. In view of this point, a model-based strategy will be proposed to improve the performance of real-time vibration fault detection.

According to the discrete model (7), the sensor system considering fault input is modeled as

$$\begin{cases} x_{k+1} = Ax_k + D_f f(x_k) + B u_k + D d_k \\ y_{k+1} = Cx_{k+1} \end{cases} \quad (24)$$

Here, u_k is known excitation input and d_k is unknown fault input caused by the changes or damages to the monitored object structure. These changes or damages may be slowly time-varying or fast time-varying. The weak fault with fast time-varying characteristic widely exists in the practical fault diagnosis of mechanical equipment. Especially for the incipient fault of mechanical equipment, the fault signal is very weak and always submerged in the strong vibration. Due to the variance of operation condition and inherent nonlinearity of equipment, this weak fault is nonstationary signal and has fast time-varying characteristic. In general, the prior knowledge on the fast time-varying fault cannot be obtained in advance. By taking full advantage of the real-time absolute motion measurement and model-based detection method, a real-time fault detection can be simultaneously realized for both weak faults of slowly time-varying and fast time-varying. Matrices A, B, D_f and function $f(x_k)$ are defined in (7). Sensor matrix and fault distribution matrix are

$$C^T = \begin{bmatrix} 1 \\ 0 \end{bmatrix}, \quad D = \begin{bmatrix} 0 \\ T_s \end{bmatrix} \quad (25)$$

To detect the fault input, inspired by Sayyaddelshad and Gustafsson [28], a full order nonlinear observer depicted in Fig.4 is constructed

$$\begin{aligned} z_{k+1} &= N z_k + R u_k + L y_k + M D_f f(\hat{x}_k) \\ \hat{x}_k &= z_k - E y_k \end{aligned} \quad (26)$$

Vector $z_k \in \mathbb{R}^2$ and $\hat{x}_k$ is the estimation of x_k. $f(\hat{x}_k)$ is a nonlinear term having the same structure as $f(x_k)$ defined in the system (7). The input to the observer is the known excitation u_k, which can be generated from a shaker or other vibration sources. The residual signal r_k is generated from the difference between the measurement of absolute motion y_k and its estimation $\hat{y}_k$. Observer matrices N, R, L and M with appropriate dimensions are the unknown parameters to be determined.

A fault detection observer for system (24) is required to satisfy the following conditions: 1) the error dynamics

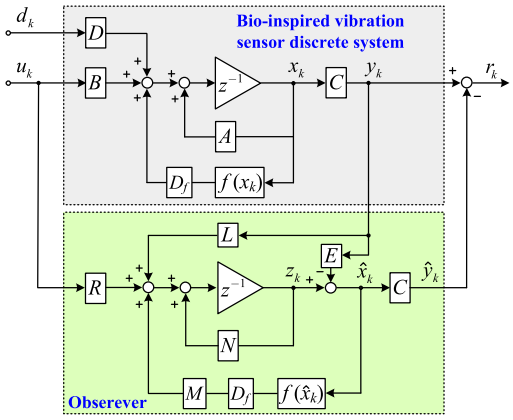

FIGURE 4. Observer based fault detection block diagram.

$\tilde{x}_k = x_k - \hat{x}_k$ asymptotically converge to zero as $k \to \infty$ in fault-free case, i.e., $r_k \to 0$; 2) the inconsistencies between the fault-free case and faulty case can be reflected on the residual signal r_k.

It is noted that the nonlinear function $f(x_k)$ belongs to $\mathcal{C}^1$, i.e., its first-derivative exists and is continuous. On the other hand, the state variables are bounded (the range of absolute motion cannot exceed the length of the road and the energy of the input is bounded). Thus, nonlinear function $f(x_k)$ is locally Lipschitz. The following condition holds

$$\|f(x_l) - f(x_u)\| \leq \tau \|x_l - x_u\|, \quad \forall x_l,\ x_u \in \Omega \tag{27}$$

where $\|\cdot\|$ is 2-norm operator, Ω is the bounded operating region of state variables and $\tau \geq 0$ is the Lipschitz constant. Due to $f(x_k) \in \mathcal{C}^1$, the Lipschitz constant can be determined through calculating its derivative

$$\tau \geq \sup_{x_k \in \Omega} \{\| \frac{\partial f(x_k)}{\partial x_k} \|\} \tag{28}$$

Theorem 1: For given Lipschitz constant τ, if there exist matrices $P > 0$, $\bar{E}$ and $\bar{X}$ with appropriate dimensions satisfying the following conditions: $MD \neq 0$ and

$$\begin{bmatrix} \tau^2 I - P & 0 & A^T P + A^T C^T \bar{E}^T - C^T \bar{X}^T \\ * & -I & D_f^T P + D_f^T C^T \bar{E}^T \\ * & * & -P \end{bmatrix} < 0 \tag{29}$$

then (26) is a fault detection observer for the sensor system (24). Moreover, the observer parameters are given by

$$\begin{aligned} E &= P^{-1}\bar{E}, \quad X = P^{-1}\bar{X} \\ M &= I + EC, \quad R = MB \\ N &= MA - XC, \quad L = X(I + CE) - MAE \end{aligned} \tag{30}$$

The proof of this theorem can be found in Appendix B.

Remark 4: According to the proof in Appendix B, matrix M is expressed as $M = I + EC$. From (25), it is obtained that $MD = D + ECD = D \neq 0$. Thus, the condition $MD \neq 0$ in Theorem 1 is always satisfied for sensor system (24).

Conforming to the Theorem 1, the fault detection observer design problem can be solved by checking the feasibility of condition (29). If feasible, a suitable fault detection observer is yielded from (30). Apart from the unknown matrices P, $\bar{E}$, and $\bar{X}$, Lipschitz constant τ is another important parameter deciding the existence of feasible solution. In general, the Lipschitz constant τ cannot be arbitrarily large. Referring to the Theorem 1, solution to give the maximum admissible Lipschitz constant satisfying the condition (29), which represents the conservativeness of the fault detection observer design, is stated as follows.

Corollary 1: The maximum admissible Lipschitz constant τ such that the condition (29) holds can be obtained via the optimal solution of the following convex optimization problem:

$$\begin{aligned} &\min_{P,\bar{E},\bar{X}} \ \lambda \\ &\text{subject to (31)}, \quad \text{with } \lambda \equiv \frac{1}{\tau^2} > 0 \\ &\begin{bmatrix} -P & 0 & A^T P + A^T C^T \bar{E}^T - C^T \bar{X}^T & I \\ * & -I & D_f^T P + D_f^T C^T \bar{E}^T & 0 \\ * & * & -P & 0 \\ * & * & * & -\lambda I \end{bmatrix} < 0 \end{aligned} \tag{31}$$

The maximum admissible Lipschitz constant is given by $\tau^* = \sqrt{\frac{1}{\lambda^*}}$, where λ^* is the optimal value of λ, and the corresponding fault detection observer is recovered from (30).

Based on the designed fault detection observer from Theorem 1, the residual signal is obtained $r_k = y_k - C\hat{x}_k$. In order to identify the fault signal exactly from the residual signal r_k, a residual evaluation strategy consisting of the evaluation function, threshold and fault classification is proposed [29], [30]. Here, choose a sliding time-window norm as the evaluation function

$$J(r_k) = \frac{1}{\Delta k} \sqrt{\sum_{k=k_0}^{k_n} r_k^T r_k}, \quad \Delta k = k_n - k_0 + 1 \tag{32}$$

The corresponding threshold is designed

$$J_{\text{th}} = \mu \sup_{\Delta_k = 0} J(r_k) + \beta \tag{33}$$

Positive scalars $\mu \geq 1$ and $\beta \geq 0$ are weight coefficients. The fault detection sensitivity can be altered by adjusting the weight coefficients and sliding time-window length. According to the evaluation function (32) and threshold (33), the logic of fault detection is

$$\begin{cases} J(r_k) \geq J_{\text{th}} \Longrightarrow \text{Fault Occurs} \Longrightarrow \text{Alarm} \\ J(r_k) < J_{\text{th}} \Longrightarrow \text{Fault Free} \end{cases} \tag{34}$$

The difference of absolute motion between the fault-free case and faulty case has been given by the residual signal r_k. Thus, when a fault detection alarm is triggered, it is possible to conduct a fault level evaluation by analyzing the envelope of residual signal r_k. Furthermore, the type of fault can be identified from the fault level. But in this paper, only simple

fault detection is considered, the identification of fault level and type will not be included.

The fault detection method has been summarized as an algorithm given in Algorithm 2.

Algorithm 2 Algorithm for Fault Detection

1: Choose a appropriate τ from (28).

2: Solve the following convex optimization problem to obtain a feasible solution P, $\bar{E}$, and $\bar{X}$.

$$\text{s.t. } P > 0, \quad (29)$$
$$\text{for } P, \bar{E}, \bar{X}, A, C \text{ and } \tau$$

3: Calculate the fault detection observer parameters as (30).

4: Implement the fault detection observer and output r_k.

5: Design the threshold J_{th} from (33) at fault-free case.

6: If the evaluation function $J(r_k) \geq J_{\text{th}}$ is satisfied, then trigger alarm and even classify fault level from residual r_k.

Remark 5: Algorithm 2 presents a real-time fault detection strategy which is implemented by applying the bio-inspired vibration sensor and constructing the fault detection observer. Compared with acceleration signal, sometimes it is more reasonable to use the absolute motion to describe the degree of structure damage caused by fault [31]. Because the absolute motion can given more information on the structural deformation, which can be used to analyze the operating condition and health status of the monitored object.

V. RESULTS

In this section, the first stage will estimate the damping coefficient by applying the parameter estimation method in Algorithm 1. Then, based on the obtained comparatively exact model of the sensor system, the second stage will construct the model-based fault detection as depicted in Algorithm 2 and an experiment will be conducted to demonstrate this fault detection method. The parameter values are given in Table 3.

TABLE 3. The bio-inspired sensor parameters.

Symbol	Description	Value
m	loading mass (kg)	0.21
L	length of rod (m)	0.10
α	initial angle (rad)	0.13π
n	number of layers	3
k_h	spring stiffness (N/m)	390
T_s	sampling period (s)	0.001

A. PARAMETER ESTIMATION

In this experiment, the input excitation is generated from a shaker. Here, a sinusoid excitation with 8Hz frequency is selected as input. The shaker requires a short period to generate the standard sinusoid signal. Thus the input excitation during the initial period is not a standard sinusoid excitation

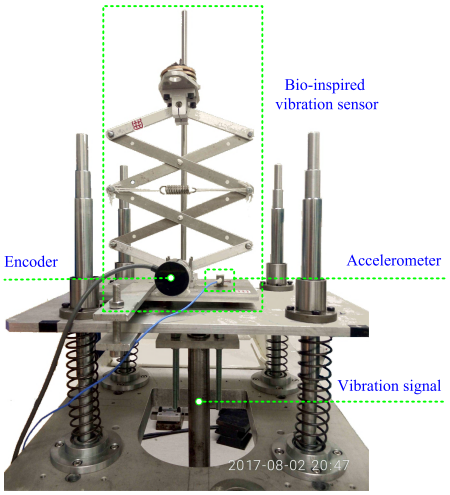

FIGURE 5. The bio-inspired sensor prototype system and experimental platform.

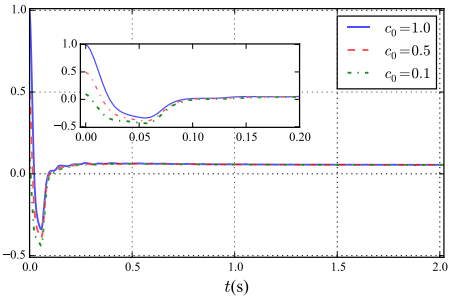

FIGURE 6. Parameter estimation result with different initial guess.

but a sinusoid-like signal. State variables and input signal are measured by using laser, encoder and accelerometer.

For the Algorithm 1, three different initial guesses for rotational damping coefficient are considered: $c_0 = 1.0$, $c_0 = 0.5$ and $c_0 = 0.1$. As depicted in Fig. 6, all the estimation results converge to a constant value at almost 0.052 after $t = 0.5$ s, which indicates that Algorithm 1 is not sensitive to the initial value. Thus, the estimation value of rotational damping coefficient is $c = 0.052$. State variables and error dynamics are shown in Fig. 7. x_k^1 and x_k^2 are the real measurement. $\hat{x}_k^1$ and $\hat{x}_k^2$ are the system state from the predictor. e_k^1 and e_k^2 are the error dynamics between the real measurement and predictor. The errors may come from the unmodeled dynamics and disturbances. It can be observed that the state variables of model are in basic agreement with the real measurement, which demonstrates the effectiveness of Algorithm 1.

B. FAULT DETECTION

By applying Theorem 1 with a Lipschitz constant $\tau = 80$, the parameters of fault detection observer are obtained

$$N = \begin{bmatrix} 0 & 0.0001 \\ -0.0002 & 0.2859 \end{bmatrix}, \quad R = \begin{bmatrix} 0 \\ -0.001 \end{bmatrix}$$
$$M = \begin{bmatrix} 0.0847 & 0 \\ -681.5633 & 1 \end{bmatrix}, \quad L = \begin{bmatrix} 0.1424 \\ -486.7297 \end{bmatrix}$$
$$E = \begin{bmatrix} -0.9153 \\ -681.5633 \end{bmatrix} \quad (35)$$

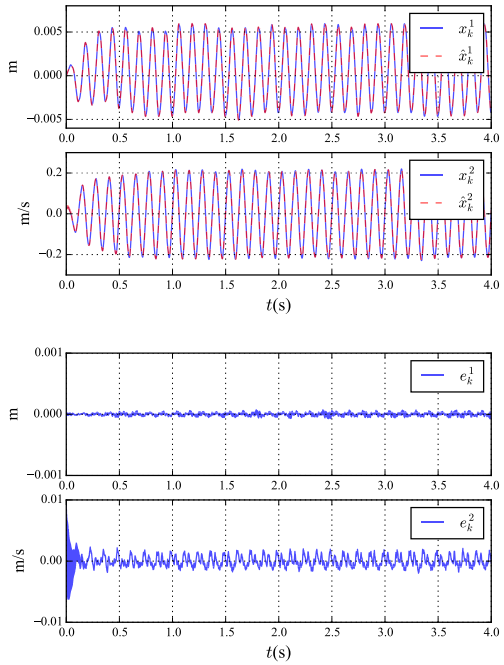

FIGURE 7. System state and error dynamics.

TABLE 4. Comparison of the maximum admissible Lipschitz constant.

Method	The maximum value of τ
Method in Ref. [28]	301.2329
Corollary 1 in this paper	703.5384

The conservativeness of the fault detection observer design method proposed in this paper is evaluated by calculating the maximum admissible Lipschitz constant. As shown in Table 4, $\tau_{\max}$ obtained by Corollary 1 of this paper is larger than that obtained in [28]. To further illustrate the conservativeness on the structure parameters, the maximum admissible Lipschitz constant with different spring stiffness $k_h \in [380\ 400]$ and loading mass $m \in [0.18\ 0.25]$ is depicted in Fig. 8, from which it can be easily seen that Corollary 1 can always provide larger $\tau_{\max}$ than that of [28] on the whole given parameter space. Thus, the fault detection observer design method of this paper is less conservative. And the design flexibility can benefit from the low conservative method.

This fault detection experiment is conducted on the vibration platform as shown in Fig. 5. Excitation input is a sinusoid signal with 8Hz generated from shaker. The absolute vibration motion is measured through the optical encoder. The relationship of vibration motion and rotation angle measured by encoder has been presented in (5). The input signal is measured by the accelerometer. Fig. 9 shows the measurement of absolute vibration motion under the fault free case and faulty case. For faulty case, fault signal occurs at $t \in [6.65\ 6.75]$ s.

From the sensor parameters in Table 3, the natural frequency can be approximated as $f_0 \approx 0.98$ Hz by (4). According to the motion transmissibility property of the bio-inspired

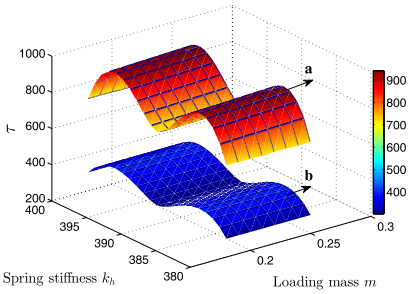

FIGURE 8. The maximum admissible Lipschitz constant with different m and k_h, a: Corollary 1 in this paper, b: Method in Ref. [28].

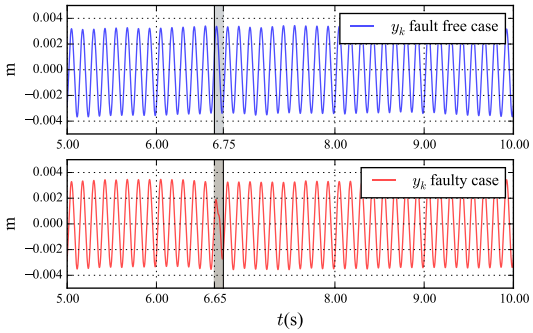

FIGURE 9. Absolute vibration motion y_k.

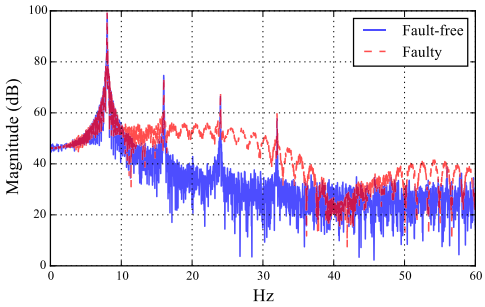

FIGURE 10. Spectrum comparison of y_k.

vibration sensor, when the frequency of base excitation is larger than $\sqrt{2}$ times the natural frequency, the sensor has a high-accuracy measurement of absolute motion by using y_r instead of y_a. Thus, the absolute motion can be given through measuring y_k. Next, we will make use of the measured absolute motion and fault detection observer (35) to construct a fault detection system.

As depicted in Fig. 4, the residual signal r_k is generated by the difference between absolute motion y_k and its estimation $\hat{y}_k$. Based on the fault detection observer (35), the estimation of y_k is expressed as $\hat{y}_k = C\hat{x}_k$. The responses of residual signal r_k and evaluation function $J(r_k)$ are shown in Fig. 11. The threshold of fault detection system here is set as $J_{\text{th}} = 1.032 \times 10^{-4}$. Spectrum comparison of y_k between fault-free and faulty cases is shown in Fig. 10, from which it is clear that the characteristic frequency of the fault signal is covered by the excitation input and its harmonics. Due to the

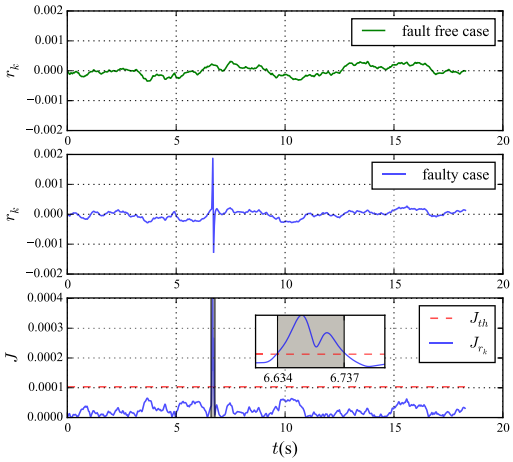

FIGURE 11. Residual response and fault detection result.

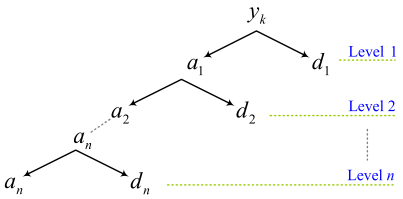

FIGURE 12. *n* levels multi-resolution wavelet decomposition.

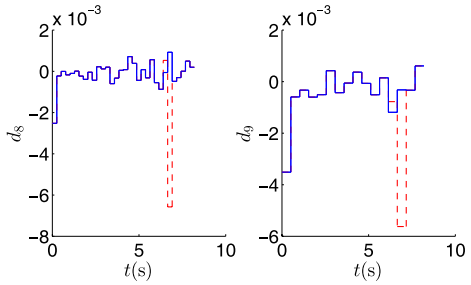

FIGURE 13. Parts of wavelet decomposition results (blue solid line is fault-free case, red dotted line is faulty case).

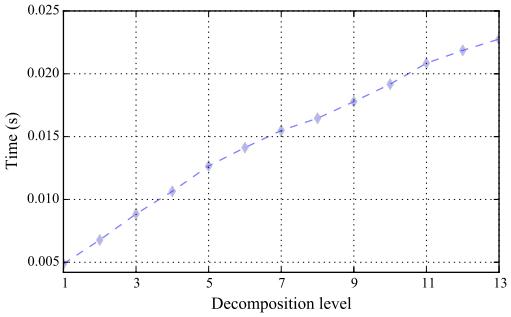

FIGURE 14. Computational time for different decomposition level.

fast time-varying characteristic, the spectrum power of faulty case in some high frequency is stronger than that of fault-free case, for example, from 10 Hz to 40 Hz. But it is difficult to locate the fast time-varying fault by using the simple spectrum analysis. The detection of the fast time-varying fault can be realized by adopting some advanced and complicated methods, such as the short time Fourier transform (STFT) [6] and the wavelet-based method [7]. The prior knowledge on the fast time-varying fault is generally unavailable. In order to obtain a high spectral resolution, the STFT method needs a long acquisition time, which will increase the computational complexity and degrade the real-time performance. Wavelet-based method requires a precise adjustment of the bands of decomposition to locate the fault signal. Thus, real-time and accuracy performance of fault detection is difficult to be simultaneously guaranteed by using the frequency-based or wavelet-based fault detection methods, especially for the weak fault with fast time-varying.

To further demonstrate the advantage of the proposed fault detection approach, multi-resolution wavelet-based method in [7] is applied to analyse the measured signal y_k. The entire decomposition procedure of multi-resolution wavelet with n levels is illustrated in Fig. 12. For the convenience of conducting wavelet decomposition, only $2^{13} = 8192$ points during $t \in [0, 8.192)$ s are selected. Here the decomposition level is $n = 13$. Parts of wavelet decomposition results (d_8, and d_9) are shown in Fig. 13. Obviously, the fault can be located by detecting the singular value of the decomposition components. It is worth pointing out that wavelet-based fault detection is not a real-time method, which requires the acquisition of entire off-line data. Additionally, in order to identify the singular value induced by fault signal, it is necessary to do the decomposition until the last level. Thus, as the data volume increases, the wavelet-based fault detection method will be limited to the computational complexity. Fig. 14 shows computational time for different wavelet decomposition level on a computer with Intel Core2 processors @2.20 GHz @2.20 GHz and 3.0 GB DDR2 memory. However, using the proposed fault detection strategy in Algorithm 2, on-line fault detection becomes possible. Fault detection performance is depicted in Fig. 11, where alarm is triggered and removed at $t = 6.634$ s and $t = 6.737$ s, respectively. The real fault signal occurs at $t \in [6.65\ 6.75]$ s. Table 5 shows the comparison of fault detection results between multi-resolution wavelet-based method and Algorithm 2. In level 8 decomposition, the singular value appears at $t \in [6.65\ 6.92]$ s. In level 9, the singular value arises at $t \in [6.66\ 7.17]$ s. These results illustrates that the occurrence time of fault identified by Algorithm 2 is more exact than multi-resolution wavelet-based method. For multi-resolution wavelet-based method, downsampling in decomposition is a key factor affecting the fault detection exactness. Moreover, compared with the wavelet-based method, the computational complexity of the fault detection approach in Algorithm 2 always remains constant (less than 0.001 s in one step) due to the real-time performance. Many detections and monitoring applications (e.g. building, bridge, and railway) can benefit from this real-time fault detection strategy by using the bio-inspired vibration sensor.

TABLE 5. Fault detection results.

Method	Result	Computational Time	Real-time
Wavelet (d_8)	$t \in$ [6.65 6.92] s	0.0165 s	Off-line
Wavelet (d_9)	$t \in$ [6.66 7.17] s	0.0178 s	Off-line
Algorithm 2	$t \in$ [6.63 6.74] s	$<$ 0.001 s	On-line

VI. CONCLUSION

In the paper, a novel bio-inspired vibration sensor for the real-time absolute motion measurement has been discussed, and its application for more reliable fault detection has been presented. Compared with some existing methods, the superiority of this bio-inspired sensor method lies in the following points: (1) This bio-inspired sensor has advantages of real-time performance, low cost and flexibility in comparison to traditional methods of absolute motion measurement using accelerometer and laser. For instance, the problems of error accumulation and real-time performance induced by traditional measurement method using integration of accelerometer data can be effectively eliminated. (2) By taking full advantage of the bio-inspired vibration sensor in real-time measurement of absolute vibration motion, a model-based fault detection algorithm has been proposed to cope with the on-line fault detection problem. Importantly, the fault detection method of this paper is less conservative and more reliable. (3) The detection results obtained from the on-line fault detection method of this paper are more exact and more sensitive than other methods such as the multi-resolution wavelet-based method. (4) The on-line fault detection method is very simple to implement and the computational complexity of the fault detection approach in Algorithm 2 always remains very small. Therefore, the method would have wider engineering applications, and the future work would extend the fault detection technology based on this bio-inspired vibration sensor to a series of practical applications for fault-tolerant control and health monitoring, such as vehicle active suspension system, railway, aeronautic engineering, and various civil structures like buildings, bridges, etc.

APPENDIX

A. TAYLOR SERIES EXPANSION OF THE NONLINEAR TERM IN SYSTEM (3)

Equivalent nonlinear stiffness term $k_h\, s\frac{ds}{dy_r}$

$$k_h\, s\frac{ds}{dy_r} = \frac{\tan^2\alpha\, k_h}{n^2}y_r + \frac{3\,\sin\alpha\sec^4\alpha\, k_h}{4\,Ln^3}{y_r}^2 - \frac{(4\,\sec^4\alpha - 5\,\sec^6\alpha)\,k_h}{8\,L^2n^4}{y_r}^3 + O({y_r}^4) \quad (A.1)$$

Equivalent nonlinear damping coefficient $c\,n_x(\frac{d\varphi}{dy_r})^2$

$$c\,n_x(\frac{d\varphi}{dy_r})^2 = c\,n_x\left(\frac{\sec^2\alpha}{L^2n^2} + \frac{\sin\alpha\,\sec^4\alpha}{L^3n^3}y_r - \frac{\left(3\,\sec^4\alpha - 4\sec^6\alpha\right)}{4L^4n^4}{y_r}^2 + O\left({y_r}^3\right)\right) \quad (A.2)$$

B. PROOF OF THEOREM 1

Define the error between the sensor system and observer as

$$\tilde{x}_k = x_k - \hat{x}_k = Mx_k - z_k \quad (B.1)$$

where $M = I + EC$. From (26), the error dynamics is

$$\tilde{x}_{k+1} = N_k\tilde{x}_k + (MA - LC - NM)x_k + (MB - R)u_k + MD_f(f(x_k) - f(\hat{x}_k)) + MDd_k \quad (B.2)$$

If $MA - LC - NM = 0$, $MB - R = 0$, $MD \neq 0$ and system (B.3) is asymptotically stable,

$$\tilde{x}_{k+1} = N\tilde{x}_k + MD_f(F(x_k) - F(\hat{x}_k)) \quad (B.3)$$

then observer (26) is a fault detection observer. Redefine the matrix variables as

$$N = MA - XC, \quad L = X(I + CE) - MAE \quad (B.4)$$

where $X = L + NE$. Choose a Lyapunov functional as

$$V_k = \tilde{x}_k^T P\tilde{x}_k \quad (B.5)$$

where P is a symmetric positive matrix. Asymptotic stability of system (B.3) requires

$$\Delta V_k = V_{k+1} - V_k < 0 \quad (B.6)$$

According to system (B.3)

$$\Delta V_k - (\tilde{f}_k^T\tilde{f}_k - \tau^2\tilde{x}_k^T\tilde{x}_k) = \eta_k^T\,\Pi\eta_k \quad (B.7)$$

where $\tilde{f}_k = f(x_k) - f(\hat{x}_k)$, $\eta_k^T = [\tilde{x}_k^T\ \tilde{f}_k^T]$ and

$$\Pi = \begin{bmatrix} \tau^2 I + N^T PN - P & N^T PMD_f \\ D_f^T M^T PN & D_f^T M^T PMD_f - I \end{bmatrix} \quad (B.8)$$

By noting that $\Pi < 0$ indicates $\Delta V_k < (\tilde{F}_k^T\tilde{F}_k - \tau^2\tilde{x}_k^T\tilde{x}_k)$. And then, according to Lipschitz condition (27), $\Delta V_k < 0$ is obtained. Thus the error dynamics $\tilde{x}_k = x_k - \hat{x}_k$ asymptotically converge to zero as $k \to \infty$.

However, due to the couplings of unknown matrices N, P, and M, $\Pi < 0$ is a nonlinear condition. In order to solve this problem, some linearization techniques are adopted to convert the nonlinear condition to linear case. Applying Schur complement equivalence to $\Pi < 0$ yields

$$\begin{bmatrix} \tau^2 I - P & 0 & N^T P \\ 0 & -I & D_f^T M^T P \\ PN & PMD_f & -P \end{bmatrix} < 0 \quad (B.9)$$

By substituting $N = MA - XC$ and $M = I + EC$ in (B.9), then replacing $E^T P$ and $X^T P$ with $\bar{E}^T$ and $\bar{X}^T$ respectively, (B.9) is written as the following equivalent form.

$$\begin{bmatrix} \tau^2 I - P & 0 & A^T P + A^T C^T\bar{E}^T - C^T\bar{X}^T \\ * & -I & D_f^T P + D_f^T C^T\bar{E}^T \\ * & * & -P \end{bmatrix} < 0 \quad (B.10)$$

If condition (B.10) has a feasible solution, the observer parameters are recovered as (30). This completes the proof. □

REFERENCES

[1] Y. Li, M. J. Zuo, J. Lin, and J. Liu, "Fault detection method for railway wheel flat using an adaptive multiscale morphological filter," *Mech. Syst. Signal Process.*, vol. 84, pp. 642–658, Feb. 2017.

[2] B. Garcia, J. C. Burgos, and A. M. Alonso, "Transformer tank vibration modeling as a method of detecting winding deformations-part I: Theoretical foundation," *IEEE Trans. Power Del.*, vol. 21, no. 1, pp. 157–163, Jan. 2006.

[3] S. Saponara, L. Fanucci, F. Bernardo, and A. Falciani, "Predictive diagnosis of high-power transformer faults by networking vibration measuring nodes with integrated signal processing," *IEEE Trans. Instrum. Meas.*, vol. 65, no. 8, pp. 1749–1760, Aug. 2016.

[4] G. Shen, M. Stephen, Y. Xu, and W. Paul, "Theoretical and experimental analysis of bispectrum of vibration signals for fault diagnosis of gears," *Mech. Syst. Signal Process.*, vol. 43, nos. 1–2, pp. 76–89, 2014.

[5] V. K. Rai and A. R. Mohanty, "Bearing fault diagnosis using FFT of intrinsic mode functions in HilbertŰHuang transform," *Mech. Syst. Signal Process.*, vol. 21, no. 6, pp. 2607–2615, 2007.

[6] S. Nandi, T. C. Ilamparithi, S. B. Lee, and D. Hyun, "Detection of eccentricity faults in induction machines based on nameplate parameters," *IEEE Trans. Ind. Electron.*, vol. 58, no. 5, pp. 1673–1683, May 2011.

[7] A. Ziaja, I. Antoniadou, T. Barszcz, W. J. Staszewski, and K. Worden, "Fault detection in rolling element bearings using wavelet-based variance analysis and novelty detection," *J. Vibrat. Control*, vol. 22, no. 2, pp. 396–411, 2016.

[8] W. Sun, H. Pan, and H. Gao, "Filter-based adaptive vibration control for active vehicle suspensions with electrohydraulic actuators," *IEEE Trans. Veh. Technol.*, vol. 65, no. 6, pp. 4619–4626, Jun. 2016.

[9] J. Vass, R. Šmíd, R. Randall, P. Sovka, C. Cristalli, and B. Torcianti, "Avoidance of speckle noise in laser vibrometry by the use of kurtosis ratio: Application to mechanical fault diagnostics," *Mech. Syst. Signal Process.*, vol. 22, no. 3, pp. 647–671, 2008.

[10] Y. Wang, F. Li, X. Jing, and Y. Wang, "Nonlinear vibration analysis of double-layered nanoplates with different boundary conditions," *Phys. Lett. A*, vol. 379, no. 24, pp. 1532–1537, 2015.

[11] I. Kovacic, M. J. Brennan, and T. P. Waters, "A study of a nonlinear vibration isolator with a quasi-zero stiffness characteristic," *J. Sound Vibrat.*, vol. 315, no. 3, pp. 700–711, 2008.

[12] X. Sun, X. Jing, J. Xu, and L. Cheng, "Vibration isolation via a scissor-like structured platform," *J. Sound Vibrat.*, vol. 333, no. 9, pp. 2404–2420, 2014.

[13] Y. Li and D. Xu, "Vibration attenuation of high dimensional quasi-zero stiffness floating raft system," *Int. J. Mech. Sci.*, vol. 126, pp. 186–195, Jun. 2017.

[14] Y. Wang, F. Li, Y. Wang, and X. Jing, "Nonlinear responses and stability analysis of viscoelastic nanoplate resting on elastic matrix under 3:1 internal resonances," *Int. J. Mech. Sci.*, vols. 128–129, pp. 94–104, Aug. 2017.

[15] Z. Wu, X. Jing, J. Bian, F. Li, and R. Allen, "Vibration isolation by exploring bio-inspired structural nonlinearity," *Bioinspiration Biomimetics*, vol. 10, no. 5, p. 056015, 2015.

[16] X. Jing, Y. Wang, Q. Li, and X. Sun, "Design of a quasi-zero-stiffness based sensor system for the measurement of absolute vibration displacement of moving platforms," *Smart Mater. Struct.*, vol. 25, no. 9, p. 097002, 2016.

[17] H. Pan, X. Jing, W. Sun, and H. Gao, "A bioinspired dynamics-based adaptive tracking control for nonlinear suspension systems," *IEEE Trans. Control Syst. Technol.*, 2017, doi: 10.1109/TCST.2017.2699158.

[18] Q. N. Xu, K. M. Lee, H. Zhou, and H. Y. Yang, "Model-based fault detection and isolation scheme for a rudder servo system," *IEEE Trans. Ind. Electron.*, vol. 62, no. 4, pp. 2384–2396, Apr. 2015.

[19] Z. Zhao, Y. Yang, S. X. Ding, and L. Li, "Fault-tolerant control for systems with model uncertainty and multiplicative faults," *IEEE Trans. Syst., Man, Cybern., Syst.*, 2017, doi: 10.1109/TSMC.2017.2759144.

[20] H. Pan, W. Sun, H. Gao, and X. Jing, "Disturbance observer-based adaptive tracking control with actuator saturation and its application," *IEEE Trans. Autom. Sci. Eng.*, vol. 13, no. 2, pp. 868–875, Apr. 2016.

[21] Z. Zhao, Y. Yang, and Y. Zhang, "Fault tolerant control using adaptive output integral-type sliding mode," *J. Franklin Inst.*, vol. 354, no. 6, pp. 2648–2662, 2017.

[22] J. Yao, Z. Jiao, and D. Ma, "A practical nonlinear adaptive control of hydraulic servomechanisms with periodic-like disturbances," *IEEE/ASME Trans. Mechatronics*, vol. 20, no. 6, pp. 2752–2760, Dec. 2015.

[23] W. Sun, S. Tang, H. Gao, and J. Zhao, "Two time-scale tracking control of nonholonomic wheeled mobile robots," *IEEE Trans. Control Syst. Technol.*, vol. 24, no. 6, pp. 2059–2069, Nov. 2016.

[24] J. Yao, W. Deng, and Z. Jiao, "Rise-based adaptive control of hydraulic systems with asymptotic tracking," *IEEE Trans. Autom. Sci. Eng.*, vol. 14, no. 3, pp. 1524–1531, Jul. 2017.

[25] W. Sun, Y. Zhang, Y. Huang, H. Gao, and O. Kaynak, "Transient-performance-guaranteed robust adaptive control and its application to precision motion control systems," *IEEE Trans. Ind. Electron.*, vol. 63, no. 10, pp. 6510–6518, Oct. 2016.

[26] J. Yao and W. Deng, "Active disturbance rejection adaptive control of hydraulic servo systems," *IEEE Trans. Ind. Electron.*, vol. 64, no. 10, pp. 8023–8032, Oct. 2017.

[27] D. Lehrer, V. Adetola, and M. Guay, "Parameter identification methods for non-linear discrete-time systems," in *Proc. Amer. Control Conf.*, Baltimore, MD, USA, Jun. 2010, pp. 2170–2175.

[28] S. Sayyaddelshad and T. Gustafsson, "Observer design for a class of nonlinear systems subject to unknown inputs," in *Proc. Eur. Control Conf.*, Strasbourg, France, Jun. 2014, pp. 970–974.

[29] Y. Zhao, J. Lam, and H. Gao, "Fault detection for fuzzy systems with intermittent measurements," *IEEE Trans. Fuzzy Syst.*, vol. 17, no. 2, pp. 398–410, Apr. 2009.

[30] H. Li, Y. Gao, P. Shi, and H. K. Lam, "Observer-based fault detection for nonlinear systems with sensor fault and limited communication capacity," *IEEE Trans. Autom. Control*, vol. 61, no. 9, pp. 2745–2751, Sep. 2016.

[31] J. Slavić, A. Brković, and M. Boltezar, "Typical bearing-fault rating using force measurements: application to real data," *J. Vibrat. Control*, vol. 17, no. 14, pp. 2164–2174, 2011.

ZHENGCHAO LI received the B.E. degree in automation and the M.E. degree in control science and engineering from the Harbin Institute of Technology, Harbin, China, in 2012 and 2014, respectively. He is currently pursuing the Ph.D. degree in mechanical engineering with The Hong Kong Polytechnic University, Hong Kong, and the Research Institute of Intelligent Control and Systems, Harbin Institute of Technology, under the joint Ph.D. Program leading to dual awards. His current research interests include robust control and filtering, fault detection, and bioinspired system and its applications to vibration isolation or control.

XINGJIAN JING (M'13–SM'17) received the B.S. degree from Zhejiang University, Hangzhou, China, in 1998, the M.S. and Ph.D. degrees in robotics from the Shenyang Institute of Automation, Chinese Academy of Sciences, Shenyang, China, in 2001 and 2005, respectively, and the Ph.D. degree in nonlinear systems and signal processing from the Department of Automatic Control and Systems Engineering, University of Sheffield, Sheffield, U.K., in 2008.

He was a Research Fellow with the Institute of Sound and Vibration Research, University of Southampton, Southampton, U.K., where he was involved in biomedical signal processing. He joined The Hong Kong Polytechnic University, Hong Kong, as an Assistant Professor, in 2009, where he has been an Associate Professor with the Department of Mechanical Engineering, since 2015. His current research interests include nonlinear frequency domain methods, nonlinear system identification/control or signal processing, and bioinspired systems and methods, with applications to vibration isolation or control, robust control, sensor technology, energy harvesting, nonlinear fault diagnosis or information processing, and robotics.

Dr. Jing is an active reviewer for many known journals and conferences. He currently serves as the Technical Editor of the IEEE/ASME TRANSACTIONS ON MECHATRONICS, the Associate Editor of the *Mechanical Systems and Signal Processing Journal*, and an Editorial Board Member of several other international journals.

JINYONG YU received the M.S. and Ph.D. degrees in control science and engineering from the Harbin Institute of Technology, Harbin, China, in 2001 and 2010, respectively. He is currently an Associate Professor with the Department of Control Science and Engineering, Harbin Institute of Technology. His research interests include automobile electrical control and fault diagnosis.